MRS Communications (2015), 5, 211–221
© Materials Research Society, 2015
doi:10.1557/mrc.2015.39

MRS Communications

Polymers/Soft Matter Research Letter

Interwoven polymer composites via dual-electrospinning with shape memory and self-healing properties

Hossein Birjandi Nejad, Jaimee M. Robertson, and **Patrick T. Mather,** Syracuse Biomaterials Institute and Department of Biomedical and Chemical Engineering, Syracuse University, Syracuse, New York 13244, USA

Address all correspondence to Patrick T. Mather at **ptmather@syr.edu**

(Received 30 January 2015; accepted 27 May 2015)

Abstract

Material research and development is increasingly focusing on achieving specialized functionality in materials. For example, the ability to "self-heal (SH)", or naturally repair accrued damage, is attractive because it extends the lifetime of the material by increasing resistance to damaging conditions and prolonging preservation of material properties. Additionally, shape memory (SM) materials, including SM polymers, are actively considered for their ability to change shape one or more times upon application of an external stimulus. Here, we present a polymer composite, composed of poly(vinyl acetate) (PVAc) and poly(ε-caprolactone) (PCL), exhibiting both SH and SM functionalities. In fact, the SM assists in the SH ability in a process developed by our group termed, shape memory-assisted self-healing (SMASH). The advantage of the SH composite presented here is its simple fabrication. Dual-electrospinning is used to simultaneously electrospin PVAc and PCL, achieving an interwoven polymeric composite of otherwise immiscible polymers. The dual-electrospinning method facilitates precise control of the relative weight fractions of the components, and thus allows for tuning of the material properties. Upon thermal activation, damaged PVAc–PCL composites exhibited SH under a variety of testing conditions. Furthermore, the composites exhibited impressive dual and triple SM capabilities in the dry and hydrated states, respectively. Together, the commercial availability of the components and the simplicity of preparation translate to a SMASH system that could be mass produced and used as a SH coating or alone, as a packaging material.

Introduction

In practice, polymeric materials are susceptible to mechanical stress and harsh environmental conditions that can lead to the formation of microcracks and, eventually, material failure. The induced damage is challenging to detect, which makes it even more difficult, if not impossible, to repair.[1,2] Consequently, the mechanical properties of polymeric materials can be unduly compromised over time. Inspired by biological systems, "self-healing (SH)" is a fascinating and relatively young field of research that can address issues such as material failure due to the propagation of cracks, or more specifically, microcracks. SH materials exhibit the ability to repair themselves and recover functionality using the resources inherently available to them upon damage.[2,3] There are a variety of ways to classify SH materials. One categorization groups SH materials based on the particular stimulus responsible for triggering the healing mechanism, such as mechanical[4] and thermal.[5] SH composites were first introduced by White et al. by incorporating a microencapsulated healing agent and a chemical catalyst in a polymeric host.[4,6] Upon damage, the microcapsules rupture, the SH agent flows to the damaged site and polymerizes, restoring the mechanical properties of the composite.[4,6] An advantage of this approach is that it does not require any external stimulus and damage itself triggers the SH mechanism. However, a disadvantage of this method is the limited amount of available SH agent. Besides, the ruptured microcapsule itself may act as a defect in the material structure, compromising the material performance in long term. Another approach, introduced by our group, utilizes shape memory (SM)[7,8] phenomenon to prepare novel SH polymers that are capable of simultaneously closing and rebonding cracks with a simple thermal trigger.[9,10] This strategy, termed "shape memory-assisted self-healing (SMASH)", was first demonstrated in a blend system consisting of a cross-linked poly(ε-caprolactone) network (n-PCL) with interpenetrating linear poly(ε-caprolactone) (l-PCL). Such unique chemistry exhibited the SM response from the network component and a SH capacity from the linear component.[9] A drawback of this SMASH system is its low rubber modulus, which necessitates mechanical support for applications that require stiff materials. In an attempt to overcome this limitation, we report here a new polymeric SMASH system that contains a glassy polymer that leads to higher stiffness. Further, a simple electrospinning method was utilized to prepare the uniformly distributed, interwoven composites.

Electrospinning is a technique that is commonly utilized in various fields of research to fabricate fine, multiscale fibers.[11,12] In a typical electrospinning setup, a polymer solution is charged using a high-voltage power supply. As the polymer solution within the syringe becomes charged, a

https://doi.org/10.1557/mrc.2015.39 Published online by Cambridge University Press

"Taylor" cone forms at the tip of the syringe needle due to like-charge electrostatic repulsion. At a critical point, a charged jet of the polymer solution forms and is propelled towards the grounded drum.[13] Before reaching the drum, the electrostatic force overcomes the solvent surface tension force resulting in fiber draw and accelerated solvent evaporation. Dry polymer fibers are then collected on a plate, drum, or disc. Fiber properties, such as diameter and orientation, can be controlled by adjustment of the electrospinning parameters, such as voltage, flow rate, or drum rotation speed.

Recently, traditional electrospinning has been modified in many ways to improve the functionality and the versatility of the resulting nanostructures. In tissue engineering, for example, the functionalizing agents (biomolecules, such as growth factors or drugs), which are to be maintained in the fluid state, are electrospun through a coaxial capillary. The outside polymer solution encapsulates the fluid, yielding a two-layer, core–sheath fiber structure.[14] Further, composite fiber mats exhibiting a combination of properties of two or more polymers have attracted a lot of attention.[11] Liu et al. reported bicomponent TiO_2/SnO_2 nanofibers fabricated by a unique electrospinning configuration in which two distinct solutions were jetted simultaneously using a dual-spinneret assembly. The authors postulated that the side-by-side electrospinning approach provided the maximum exposure of both components and increased the surface area, leading to improved efficiency as a photocatalyst for the treatment of organic pollutants in water.[15]

Seeking to develop a one-step method to fabricate a SH systems, the present work introduces a simple dual-electrospinning method to develop composites consisting of two uniformly distributed immiscible polymers that, together, feature thermally triggered SH properties. Interwoven polymer blends with homogenous phase distribution, precise composition, and properties tuned to our specifications were fabricated. Specifically, composites consisting of poly(vinyl acetate) (PVAc) and poly(ε-caprolactone) (PCL) that feature both SH and SM functionalities were fabricated. In what follows, we discuss the preparation, morphology, and thermomechanical characterization of the composites, thus revealing their excellent potential for several industrial applications.

Experimental

Materials

N,N-dimethylformamide (DMF), chloroform, methanol, Rhodamine B, and PCL ($M_n \approx$ 70,000–90,000 g/mol, reported by supplier) were purchased from Sigma Aldrich. PVAc (M_W = 260,000 g/mol, reported by supplier) was purchased from Scientific Polymer Products. All chemicals were used as received. For electrospinning, 2 g of PVAc were dissolved in a solution containing 7.0 mL methanol and 3.0 mL DMF to obtain a 20 wt% polymer solution. About 100 mg of Rhodamine B (fluorescent dye) was mixed with the PVAc solution, turning the solution from clear and colorless to bright red. A PCL solution was prepared from 2.0 g PCL, 8.0 mL chloroform, and 2.0 mL DMF to obtain a 20 wt% polymer solution. Both solutions were stirred at room temperature (RT) with a magnetic stir bar at ~500 RPM overnight until a homogenous solution was achieved.

Dual-electrospinning setup

For this study, an electrospinning setup featuring two polymer solution delivery systems was designed.[16] The polymer solutions were contained in syringes located on opposite sides of the drum, as illustrated in Scheme S1. Having our target application in mind, we selected PVAc and PCL as the SM polymer and SH agent, respectively, for dual-electrospinning. Electrospinning parameters for each polymer solution were set independently:

PVAc: 13.0 kV applied voltage and 8 cm tip of the needle to collector distance.
PCL: 12.0 kV applied voltage and 10 cm tip of the needle to collector distance.

The samples are named "PVAc*x*:PCL*y*" where *x* and *y* stand for the nominal weight fraction of PVAc and PCL, respectively. The nominal weight fractions of the polymers in the composites were calculated based on the relative flow rates used for PVAc and PCL solutions during the dual-electrospinning process. Two composites, PVAc60:PCL40 and PVAc80:PCL20 were fabricated and compared to neat PVAc and PCL samples as controls.

Composite morphology and fiber distribution

Heating the fiber mat at 80 °C, which is above the characteristic glass transition temperature (T_g) and melting transition temperature (T_m) of PVAc and PCL, respectively, allows the chains to reconfigure to a relaxed, lower energy state and melts the PCL fibers to a film. The heating step also results in significant shrinkage in size, which aided in filling the voids of the porous fiber mat to form a film (see Results and discussions section). Hereafter, the as-spun and heated samples are called fibers and films, respectively. The morphologies of the composites pre- and post-heating (fibers and films) were studied using a JEOL JSM-5600 scanning electron microscope (SEM). Prior to imaging, samples were sputter coated (Denton Vacuum-Desk II sputter coater) with gold for 45 s.

Interested in investigating fiber–fiber interactions in the dual-electrospinning process, we examined the distribution of the two fiber jets (PVAc and PCL) within the fiber mats. Ideally, both PCL and PVAc fibers should be randomly distributed within the fiber mat to assure SH at any region of the sample. To examine fiber distribution, the bright-field (under visible light) and fluorescent (under ultraviolet light with a fluorescent filter) images of the fibers were taken using a Leica DMI 4000B inverted microscope with a Leica DFC 340FX camera using a 40×/1.3 NA objective. Note that only the PVAc solution contained Rhodamine B (a fluorescent dye), so only PVAc fibers appeared under the fluorescent light.[17] Using ImageJ software, histogram stretching was carefully

https://doi.org/10.1557/mrc.2015.39 Published online by Cambridge University Press

applied to all micrographs to maximize image contrast. The bright-field images were inverted so that they had a black background, as in fluorescent images. All of these steps were conducted carefully to prevent loss of information in the micrographs. Blue and red lookup tables were then applied to the bright-field and fluorescent images, and the images were overlaid to examine the distribution of PVAc and PCL fibers in a single micrograph.

Thermomechanical properties of the composites

Thermal properties and phase behavior of the PVAc:PCL films were studied using differential scanning calorimetry (DSC), with the anticipation of pertinence to mechanical properties and SH behavior studied later. DSC experiments were conducted using a Q200 (TA Instrument) equipped with a refrigerated cooling system (RCS). Samples with masses of 3–5 mg were encapsulated in Tzero aluminum pans and were heated from −80 to 120 °C, cooled back to −80 °C, and finally heated to 120 °C. All heating rates were 10 °C/min and all cooling rates were 5 °C/min. The T_g and T_m of the samples were determined as the middle point of the step transition and the melting endothermic peak transition of the DSC second heating runs, respectively. Further, the enthalpy of melting associated with the PCL melt transition in the composites was measured to gravimetrically estimate the actual weight fractions of PVAc and PCL. To calculate the weight fraction of PCL in the composite, the ratio of the enthalpy of melting of PCL (in the composite) to that of neat PCL fibers was calculated.

Thermogravimetric analysis (TGA; TA Instruments Q500) was also utilized to support the gravimetric DSC analysis and to study the thermal stability of the composites. The TGA was employed in a high-resolution mode to better distinguish the decomposition events associated with PVAc and PCL. A maximum heating rate of 20 °C/min, a resolution number of 4, and a sensitivity value of 1 were used for this study. All samples were heated to 600 °C. The weight fraction of PCL in the composite was estimated as the fraction of the sample that degraded at the temperature corresponding to PCL decomposition.

Thermomechanical properties of the films were characterized using a Q800 Dynamic Mechanical Analyzer (TA Instrument). Dogbone samples (ASTM D638 Type IV, scaled down by a factor of 4) with a typical thickness of 0.3–0.5 mm were loaded under tension and oscillatory deformation with an amplitude of 10 μm, a frequency of 1 Hz, and a "force track" (ratio of static to dynamic force) of 108%. To determine transition temperatures and rubbery plateaus of the film, the samples were equilibrated and held isothermally at −40 °C for 10 min, and then heated to 80 °C at 2 °C/min.

Microstructure characterization

To determine the microstructure of the PVAc:PCL composites (fibers and films), wide-angle x-ray scattering (WAXS) was conducted using a Rigaku S-MAX3000 (Woodlands, TX) instrument in transmission mode. A FujiFilm FLA7000 reader was used to collect the scattered x-ray diffraction patterns. A Rigaku generator (MicroMax- 002+) was employed to produce a Cu Kα radiation with a wavelength of 1.5405 Å. An accelerating voltage of 45 kV and a current of 0.88 mA were applied. The distance between sample and image plate was fixed at 122.7 mm for wide-angle x-ray scattering collection. The resulting scatter angles were in the range of $0° < 2\theta < 40°$. The patterns were analyzed using the SAXSgui software without background subtraction, benefiting from the fact that the whole x-ray system was under high vacuum.

SH characterization

To evaluate the ability of the film to recover from various types of mechanical damage, three different experiments were conducted. First, the SH ability of a PVAc60:PCL40 film was assessed qualitatively by applying a cross-shaped cut on the surface of the sample. The damaged sample was then thermally mended (or "self-healed") by heating isothermally at 75 °C for 10 min. The SH behavior was further investigated following a method developed by Yamaguchi et al..[18] First, the top surface of a rectangular sample (23 mm length, 4.2 mm width, and 0.8 mm thickness) was notched. The crack was then opened/propagated by pushing the two ends of the sample against a cylindrical object (9.0 mm in diameter). This action almost broke the sample in half, but a thin lesion on the back side held the two halves together. The sample was then heated to 75 °C, held isothermally for 10 min, and then cooled to RT to observe thermal mending qualitatively. Finally, a third, quantitative, SH experiment was conducted using the deeply double-edge notched tensile (DDENT) geometry employed for fracture testing of polymeric films.[9,19,20] A dogbone (ASTM D638-03 Type I, scaled down by a factor of 3) shaped PVAc60:PCL40 (40% PCL was previously found to be the optimal loading level for efficient SH in another system[9]) film with a typical thickness of 0.8–1.0 mm and a PVAc (as a control with no PCL, i.e. SH agent) film were notched using a custom-made cutter to create two collinear, gauge-centered edge-cracks that were 0.5 mm long on each side of the dogbone neck. The gauge length for such specimen was 16.67 mm. To controllably propagate the damage, the notched sample was then stretched at a slow rate (10 μm/s) to 5.0 mm (corresponding to 30% strain) using a TST350 Linkam Tensile Stress Testing Stage (Linkam Scientific Instruments, Ltd.) with a 200 N load cell. The unconstrained, damaged sample was then heated to 75 °C and held isothermal for 10 min to initiate thermal mending. To evaluate the crack propagation and SH processes, micrographs of notched, stretched, and self-healed samples were taken using a Zeiss Discovery V8 stereo microscope with a QIMAGING (QICAM FAST1394) CCD camera. SH was assessed by comparing the mechanical properties of virgin, damaged, and healed samples. SH efficiency was defined as

$$\eta(\%) = \frac{F^{\mathrm{Max}}_{\mathrm{Healed}}}{F^{\mathrm{Max}}_{\mathrm{Virgin}}} \times 100, \quad (1)$$

https://doi.org/10.1557/mrc.2015.39 Published online by Cambridge University Press

where the virgin (F^{Max}_{Virgin}) and healed (F^{Max}_{Healed}) peak loads were obtained from the force versus displacement curves recorded for the virgin and healed samples stretched in the Linkam tensile stage. For a completely healed sample, the force versus displacement curves should be identical to that of the virgin sample and thus 100% SH efficiency.

Triple SM characterization of the hydrated composite

One approach to develop triple SM materials is to develop composites featuring two well-separated thermal transitions.[21] The T_g of PVAc decreases to ~16 °C upon equilibrium plasticization with water, and consequently, the water-soaked PVAc:PCL film has a T_g about 16 °C and a T_m (from PCL) around 55 °C, making it an appropriate candidate for triple SM behavior. To characterize this material, dual SM properties of the dry film were first examined. A rectangular PVAc80:PCL20 film (21.0 mm length, 4.0 mm width, and 0.4 mm thickness) was heated to 80 °C, deformed into a spiral shape by wrapping around a glass rod with a diameter of 5 mm, held isothermal for 5 min, and quenched by placing in a freezer at −17 °C for 10 min. For recovery, the sample was heated isothermally in an oven at 80 °C. To qualitatively assess the triple SM behavior of the film, a rectangular piece of PVAc80:PCL20 film was immersed in water overnight to assure complete hydration. Then, the sample was curled to a "C" shape (temporary shape 1) in an 80 °C water bath and fixed immediately by quenching in an ice/water bath. For the second temporary shape, the sample was rolled on itself to a compact form in a water bath at RT and quenched in an ice/water bath. For recovery, the sample was sequentially immersed in water at RT for 10 min and then heated to 80 °C. It is noted that triple SM properties are not exhibited in the dry composite, since the transition temperatures of the PVAc and PCL are found in a narrow temperature window.

Mechanical properties of hydrated versus dry films

The mechanical properties of PVAc and PVAc80:PCL20 films, in both the dry and wet states, were studied using the same Linkam TST-350 tensile tester at RT. Dogbone-shaped samples (ASTM Standard D638 Type IV, scaled down by a factor of 4) with a typical thickness of 0.3–0.5 mm were stretched at 50 μm/s at RT to failure. For the dry and hydrated samples, a 200 N (0.1 N resolution) and a 20 N load cell (0.01 N resolution) were used, respectively. Hydrated samples were immersed in water for at least 24 h prior to the experiment, and water was pipetted onto their surfaces during the experiment to maintain hydration.

Results and discussions

Dual-electrospinning setup

A schematic illustration of the dual-electrospinning setup is provided in Scheme S1. Two separate pumps, located on opposite sides of the collecting drum, controlled the flow rates of each solution. The fibers were collected on a rotating drum (diameter of ~5 cm), which rotated at 400 RPM and translated in an oscillatory fashion with a rastering amplitude of ~6 cm. An inherent advantage of this method compared with other methods, such as solvent casting or melt mixing of two immiscible polymers, is that the two different polymeric fibers are uniformly distributed and tightly interwoven with each other throughout the fiber mat. We note that in the dual-electrospinning method, the phase domains are <10 μm (since the average fiber diameter is <10 μm) and the polymer fibers are entangled with each other. Therefore, we expect that the dual-electrospinning method leads to a more uniform morphology, improving both the mechanical and the SM properties of the composites compared with other conventional methods such as solvent casting. Nevertheless, detailed comparison of dual-electrospinning method with other conventional methods such as solvent casting or extrusion, remains subject of future work. Besides, given that electrospinning conditions for each of the polymer solutions in the dual-electrospinning process were set completely independent of the other, we envision that this method is applicable to any electrospinnable polymers reported in literature, though at this point we do not have any direct proof of that.[11,13]

Composite morphology and fiber distribution

PVAc polymer chains are oriented along the length of the electrospun fibers and the polymer is in a high-energy state given the high-electric voltage applied during the electrospinning process.[22,23] Heating the fiber mat to 80 °C, which is above the characteristic T_g of the PVAc and T_m of PCL, allows PVAc chains to reconfigure to a relaxed, lower-energy state and melts the PCL fibers to yield a film. Figure 1 shows the SEM micrographs of a PVAc60:PCL40 fiber mat before and after heating. The former clearly shows a lack of orientation of the fibers and this is preserved in the consolidated films. Upon heating, the composite experiences a significant reduction in size and changes from a fiber mat to a stiff, non-porous film consisting of PVAc fibers bound by a PCL matrix, consistent with the observations in Fig. 1 (SEM images of neat PVAc and PCL fiber mats before and after heating are provided in Fig. S1). Cross-sectional SEM micrographs of the composites reveal the non-porous structure of the films post-heating as well (Fig. S2). A quantitative analysis of the heat-induced reduction in size is provided in Fig. S3. Results showed that the dual-electrospun sample (PVAc60:PCL40) has an intermediate shrinkage % value (74%) compared with the two controls [PCL (67%) and PVAc (78%) fiber mats].

Fluorescent microscopy was also utilized to investigate the distribution of the two fiber jets (PVAc and PCL) within the fiber mat. Shown in Fig. 2 are the bright-field and fluorescent images of PVAc60:PCL40 fibers and the overlay of the two micrographs. Results showed that PVAc and PCL fibers were randomly distributed in the fiber mat. This is necessary for SH purposes due to the fact that both SM polymer and SH agent have to be present at any given location in the composite to

https://doi.org/10.1557/mrc.2015.39 Published online by Cambridge University Press

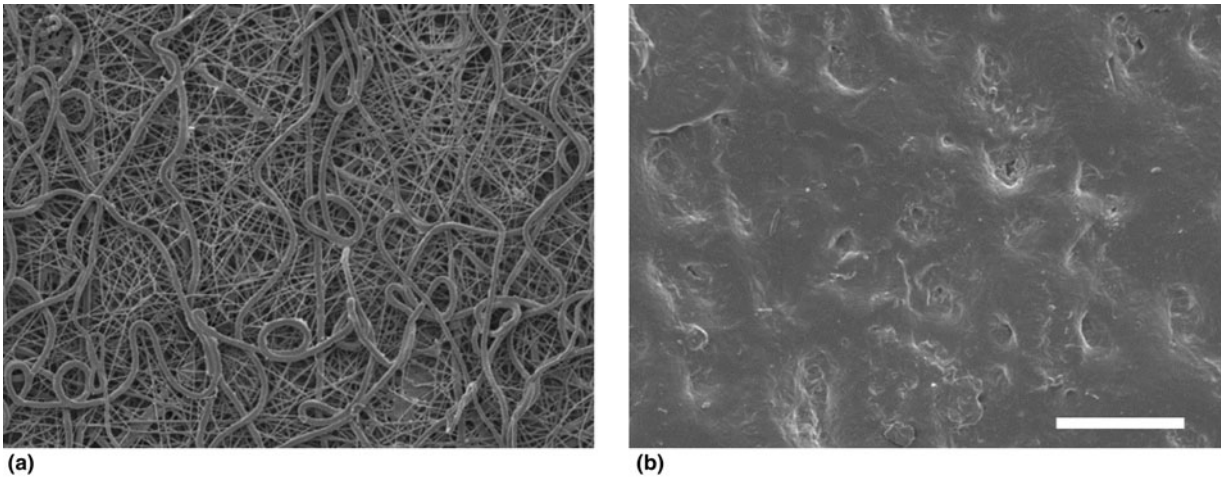


Figure 1. SEM micrographs of (a) an as spun and (b) a heated PVAc60:PCL40 fiber mat. During heating, the PVAc polymers chains reconfigure to a relaxed state and the semicrystalline PCL fibers melt and form a film resulting in significant fiber mat shrinkage. Scale bar represents 50 μm for both micrographs.

repair damage (for bright-field and fluorescent micrographs of PVAc and PCL fibers, see Fig. S4).

Thermomechanical properties

DSC experiments were conducted to study the phase transition and composition of the different PVAc:PCL films. Second cycle DSC traces of PVAc:PCL films with different compositions are provided in Fig. 3. For all PVAc:PCL films, a step-like T_g at 45 °C and a T_m at 56 °C were observed, corresponding to PVAc and PCL phases, respectively. A comparison of the first and second heating cycles of the as-spun composites revealed that the thermal processing of the fibers (i.e. heating at 80 °C) removed residual stresses imparted in the materials during dual-electrospinning (the DSC first and second heating cycles of the PVAc:PCL films are provided in Fig. S5). In the first heating cycles, the traces exhibited slight endothermic peaks in the PVAc glass transition. This peak is postulated to be due to the increased chain alignment and packing density resulting from the elongational forces experienced during electrospinning. Further, the first heat of the PVAc80:PCL20 film indicated a higher PCL T_m. Again, it is suspected that residual stresses resulting in altered microstructures caused changes in the thermal response. In both cases, after the initial first heat, the transition temperatures returned to the respective transition temperature of the neat component. Namely, the temperatures at the peak of the PCL melting transition in the composites were within 2 °C of the T_m of the neat PCL film. Therefore, based on the similarity in thermal behavior and a microstructural analysis (discussed later), we concluded that the thermal treatment used to transform the fibers to films reverted the PCL domain back to its original state; the relative crystallinity of the PCL was constant between PVAc:PCL films and neat PCL. Hence, we estimated the actual PCL weight fraction gravimetrically, by dividing the PCL enthalpy of melting in the PVAc:PCL films by that of neat PCL. Again, the relative weight fractions of PVAc and PCL fibers in the resulting dual-

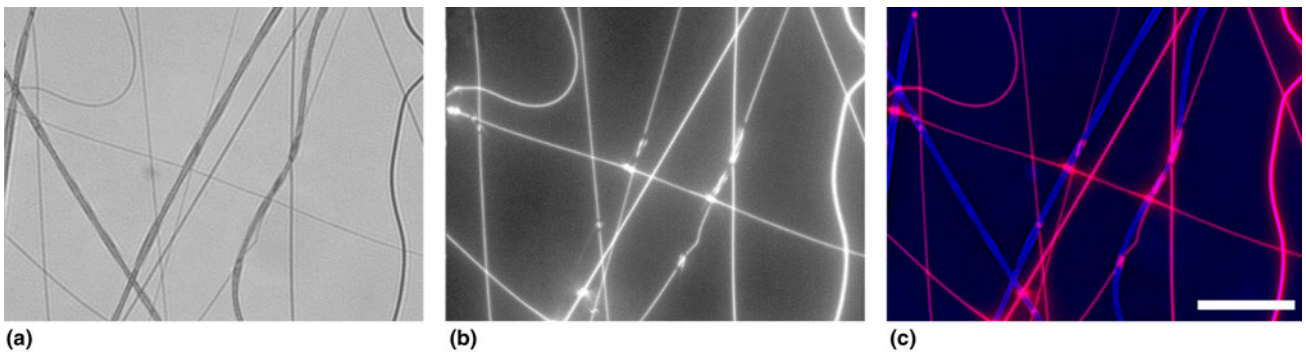


Figure 2. Representative optical micrographs showing (a) bright field, (b) fluorescent and (c) overlaid [combined (a) and (b)] images of the dual-electrospun PVAc60:PCL40 fibers. Blue and pink colors correspond to PCL and PVAc fibers, respectively. To take the images, the fibers were electrospun on a thin glass slide for ~10 s. Note that the PVAc solution contained ~0.5 wt. % of Rhodamine B. Scale bar represents 100 μm for all micrographs.

https://doi.org/10.1557/mrc.2015.39 Published online by Cambridge University Press

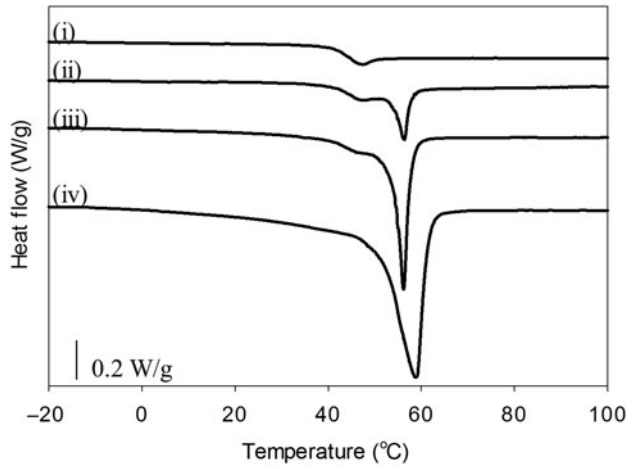


Figure 3. DSC thermograms (2nd heating cycle) of (i) PVAc, (ii) PVAc80:PCL20, (iii) PVAc60:PCL40 and (iv) PCL composites. The temperature was ramped at 10 °C/min and 5 °C/min for heating and cooling, respectively.

electrospun fiber mat can be controlled very easily by altering the initial flow rates of PVAc and PCL. Results showed that the actual PCL weight fractions were very close to the nominal PCL weight fractions in the films, assuring reliability and reproducibility of this method (Table 1).

High-resolution TGA was employed to further support the gravimetric DSC composition analysis. In high-resolution TGA, the heating rate is variable, and it depends on the instantaneous weight loss rate. If the sample weight is stable, the heating rate is high, with a maximum at the set value (20 °C/min). Shown in Fig. S6 are high-resolution TGA profiles of PVAc, PCL, PVAc80:PCL20, and PVAc60:PCL40 films. Using a 20 °C/min maximum heating rate, the PVAc was stable to about 300 °C. At this temperature, the heating rate slowed drastically, allowing the decomposition event to occur before heating again at an accelerated rate. About 70% of the PVAc mass was lost at 300 °C, and the remaining was stable until about 400 °C, at which another 26% of the mass was lost [Fig. S8 (A)]. Approximately 4% of initial mass of the PVAc remained as char at 600 °C. Note that the end of each decomposition event was defined as the peak of heating rate, i.e. where the weight loss rate in the decomposition event reaches a minimum value indicating that the decomposition event concludes (Fig. S7). Using the same method, PCL exhibited thermal stability up to about 350 °C. At this temperature, almost all of the mass was lost, and at 600 °C, only 1% of the initial mass remained [Fig. S8(B)]. To our advantage, PCL decomposition occurred separately from the PVAc decomposition events. Therefore, when the high-resolution TGA method was utilized for the PVAc:PCL composites, three decomposition events were observed, with two corresponding to PVAc decomposition and one corresponding to PCL decomposition (Fig. S6). The PCL weight fractions were estimated as the weight fractions lost during the 350 °C decomposition event given that all of PCL decomposes in this event. The measured PCL weight percentages for PVAc80:PCL20 and PVAc60:PCL40 were 20.4 and 36.5, respectively [Figs. S8(C) and S8(D)]. Notably, these values correspond very well to the nominal values and to the values obtained from the DSC analysis (Table I).

Upon hydration, the T_g of PVAc plunged to ~16 °C providing a wide window between PVAc T_g and PCL T_m, a requisite factor for triple SM properties which is discussed in detail later (for DSC of hydrated samples, see Fig. S9). The thermal properties of the films are summarized in Table I.

Thermomechanical testing was conducted to perceive the effect of composition on the viscoelastic properties of the films. This set of testing is important to provide context for the subsequent SH and SM characterizations. Tensile storage modulus (E') profiles are reported in Fig. 4 for PVAc60:PCL40, PVAc80:PCL20, and PVAc films. All compositions exhibited glassy stiffness at RT with a modulus above 1 GPa. Given that the transition temperatures of PVAc (43 °C) and PCL (56 °C) are close to each other, all compositions showed a single, combined transition (modulus drop) on-setting at ~40 °C where the storage modulus drops about three orders

Table I. Summary of the thermomechanical properties of PVAc:PCL composites in dry and hydrated states.

Sample	T_g (°C)[a]	T_m (°C)[a]	$\Delta H_{m,PCL}$ (J/g)	Actual PCL (wt%)[a]	Actual PCL (wt%)[b]
PVAc	45.2	–	–	–	–
PVAc-hydrated	16.5	–	–	–	–
PVAc60:PCL40	44.4	56.2	17.8	38.2	36.5
PVAc80:PCL20	43.0	55.1	10.1	21.5	20.4
PVAc80:PCL20-hydrated	15.5	52.0	–	–	–
PCL	–	58.8	46.6	–	–

–, Does not apply.
[a]Measured by DSC.
[b]Measured by high-resolution TGA (for TGA results, see Figs. S6–S8).

https://doi.org/10.1557/mrc.2015.39 Published online by Cambridge University Press

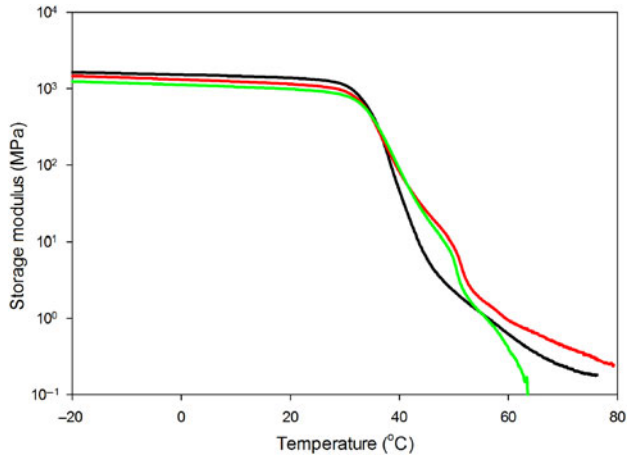


Figure 4. Storage modulus (E) traces of (green line) PVAc60:PCL40 film, (red line) PVAc80:PCL20 film and (black line) PVAc film.

of magnitude. The loss tangent [tan(δ)] profiles for PVAc60:PCL40 and PVAc80:PCL20 however showed double peaks, indicative of both PVAc T_g and PCL T_m which was in agreement with DSC results (see Fig. S10). Therefore, we anticipated that a simple heating step above both transitions (i.e. 75 °C) would simultaneously trigger both the SM response of the PVAc phase and melting of the PCL phase, yielding the two-step SMASH mechanism.

At 25 °C, the storage moduli of the PVAc:PCL composites were about five times higher than the corresponding composites with the same SH agent wt% in the first SMASH system reported by our group.[9] The superior mechanical properties of the PVAc:PCL composites satisfy the requirements for applications that require stiff materials. A comparison between the thermomechanical properties of the current composite system (dual-electrospun PVAc:PCL interwoven films) and the first SMASH system reported by our group[9] [crosslinked PCL (n-PCL)/linear (l-PCL) interpenetrating network] is provided in Table S1.

Note that above its melting temperature, PCL becomes a viscous liquid that flows, yielding alteration in sample geometry. The storage modulus (E') trace of PCL as a function of temperature is provided in Fig. S11, showing a sharp drop in storage modulus as PCL goes through the melting transition and transforms from a solid to a liquid. These results indicate that PCL by itself cannot hold any applied stress and requires a second phase (PVAc in our case) for mechanical support to keep the integrity of the composite when heated above the PCL melting transition. In the presence of PVAc, PVAc80:PCL20 and PVAc60:PCL40 films showed soft rubber characteristics and had storage modulus values of 0.8 and 0.3 MPa, respectively at 60 °C.

Microstructure characterization

The microphase morphologies of PVAc60:PCL40, PVAc, and PCL as-spun fiber mats and post-heating films were characterized using WAXS. Shown in Fig. 5 are the two-dimensional (2D) WAXS patterns (corresponding diffractograms are shown in Fig. S12). The PVAc scattering pattern [Fig. 5(b)]

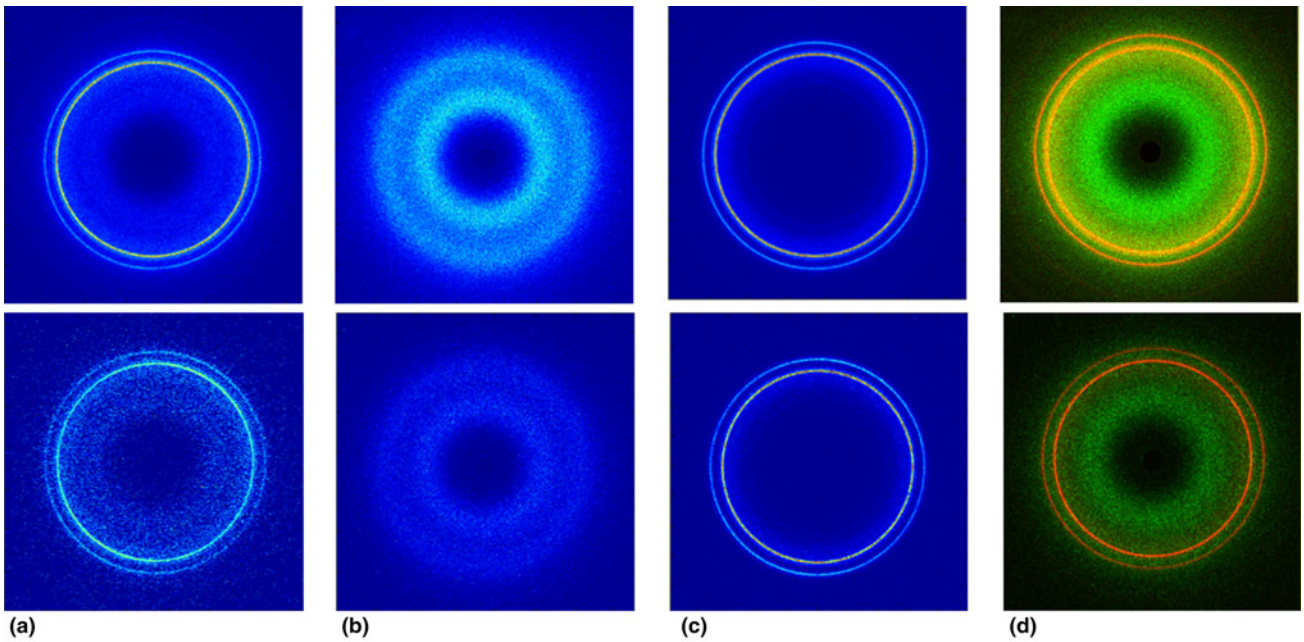


Figure 5. Wide angle x-ray scattering (WAXS) patterns of (a) PVAc60:PCL40, (b) PVAc and (c) PCL. The top and bottom rows represent films and fiber mats, respectively. Shown in (d) are the overlaid patterns of PVAc (b) and PCL (c), which are in good agreement with PVAc60:PCL40 (a) results. The x-ray wavelength (λ) is 1.5405 Å.

https://doi.org/10.1557/mrc.2015.39 Published online by Cambridge University Press

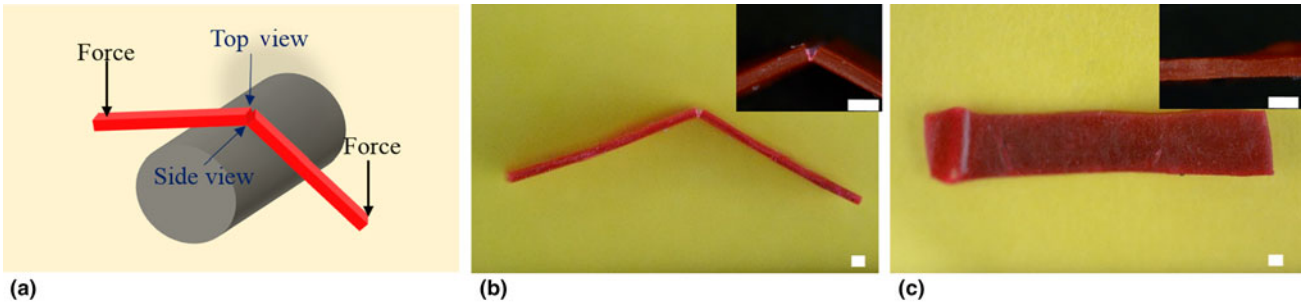


Figure 6. (a) Schematic illustration of the crack opening method. The surface of the sample was first cleaved by a fresh razor blade. The sample was then bent on a cylindrical rod to propagate the crack. Shown in (b) and (c) are photographs of the damaged and self-healed samples, respectively. Insets present the zoomed in stereo micrographs of the damaged and self-healed samples. All scale bars denote 1 mm.

showed two broad halos with no preferred orientation, which is indicative of the amorphous and isotropic structure of the polymer. The PCL pattern, in contrast, showed sharp Debye–Scherrer rings corresponding to diffraction from crystalline planes of the PCL crystallites [Fig. 5(c)]. As expected, the PVAc60:PCL40 composite showed a combination of the aforementioned structures. In the WAXS pattern for this composite [Fig. 5(a)], a broad halo and two sharp rings were present, corresponding to amorphous PVAc and semi-crystalline PCL phase, respectively. WAXS patterns of neat PVAc and PCL were overlaid, and the compiled pattern predictably matched that of the composite [Fig. 5(d)]. It is noted that the WAXS pattern of fiber mats featured lower intensity values for the same exposure time than those of films due to their reduced thickness relative to their counterpart solid films.

SH characterization

For successful SH, the crack surfaces of a damaged article should close and rebond, restoring mechanical integrity in doing so. In the present system, the healing agent (PCL) transitions to a relatively low-viscosity liquid when heated above its T_m and is therefore capable of wetting the damaged area and "gluing" the surfaces together upon recrystallization.[9] Our candidate composition was PVAc60:PCL40 given that a previous report by Rodriguez et al. on SMASH composites revealed that to achieve complete healing, the weight fraction of the healing agent needed to be at least 25 wt.%.[9] To characterize the ability of the composites to recover their initial properties upon damage, we conducted the SH experiments described in the Experimental section.

In the first experiment, the SH ability of a PVAc60:PCL40 film was assessed by scoring the samples with a cross-shaped cut on the surface of the sample, as shown in Fig. S13(A). Upon thermal mending, the entire scar gratifyingly disappeared [Fig. S13(B)]. In this case, however, the sample surface had been damaged and more experiments were needed to study if the bulk of the sample showed similar features as we now discuss. Consistent with the mechanically isotropic nature of the samples, we did not observe a direction-dependence for this remarkable behavior.

The self-repairing behavior was further investigated by inducing relatively more severe damage to the sample. First, the top surface of the sample was notched and the crack was then opened by bending the sample onto a column until it cleaved as illustrated in Figs. 6(a) and 6(b). The healed sample, mended isothermally at 75 °C for 10 min, is shown in Fig. 6(c). To have complete SH, two mechanisms are required: (1) The SM effect should unbend the sample and bring the two cracked surfaces together; and (2) the SH agent should diffuse to the damage site, tackify, and consequently rebond the crack surfaces. The healability of the sample was impressive, given that the sample not only returned to its original shape, but also the initial crack was mended.

Lastly, SH efficiency was determined by comparing the peak loads achieved during tensile testing of the virgin and healed states of samples damaged with the DDENT. Each sample in its virgin, damaged, and healed states was stretched above its yield point. Shown in Fig. 7(I) are the micrographs of a virgin, notched, stretched, and thermally mended sample. Upon heating to 75 °C and holding for 10 min, this sample showed that propagated crack damage was completely mended. By heating above the T_g of the PVAc phase, the SM mechanism was triggered, assisting in crack closure. Meanwhile, heating above the T_m of the PCL phase allowed the crack surfaces to rebond. Force versus displacement curves for such experiment are shown in Fig. 7(II), noting that tensile stress is ill-defined for this geometry and, so, not reported. We observed that the peak loads associated with the initial deformations were higher than the peak loads of damaged samples (samples that were notched and stretched prior to the test). However, thermally mended samples showed peak loads similar to the virgin state with a SH efficiency of 99.0%. It is notable that both virgin and healed samples showed similar force-displacement profiles and did not break in the monitored 5.00 mm displacement range. In the absence of PCL (SH agent), however, the damaged PVAc film did not recover its original properties after heating. The PVAc film had a relatively lower SH efficiency

https://doi.org/10.1557/mrc.2015.39 Published online by Cambridge University Press

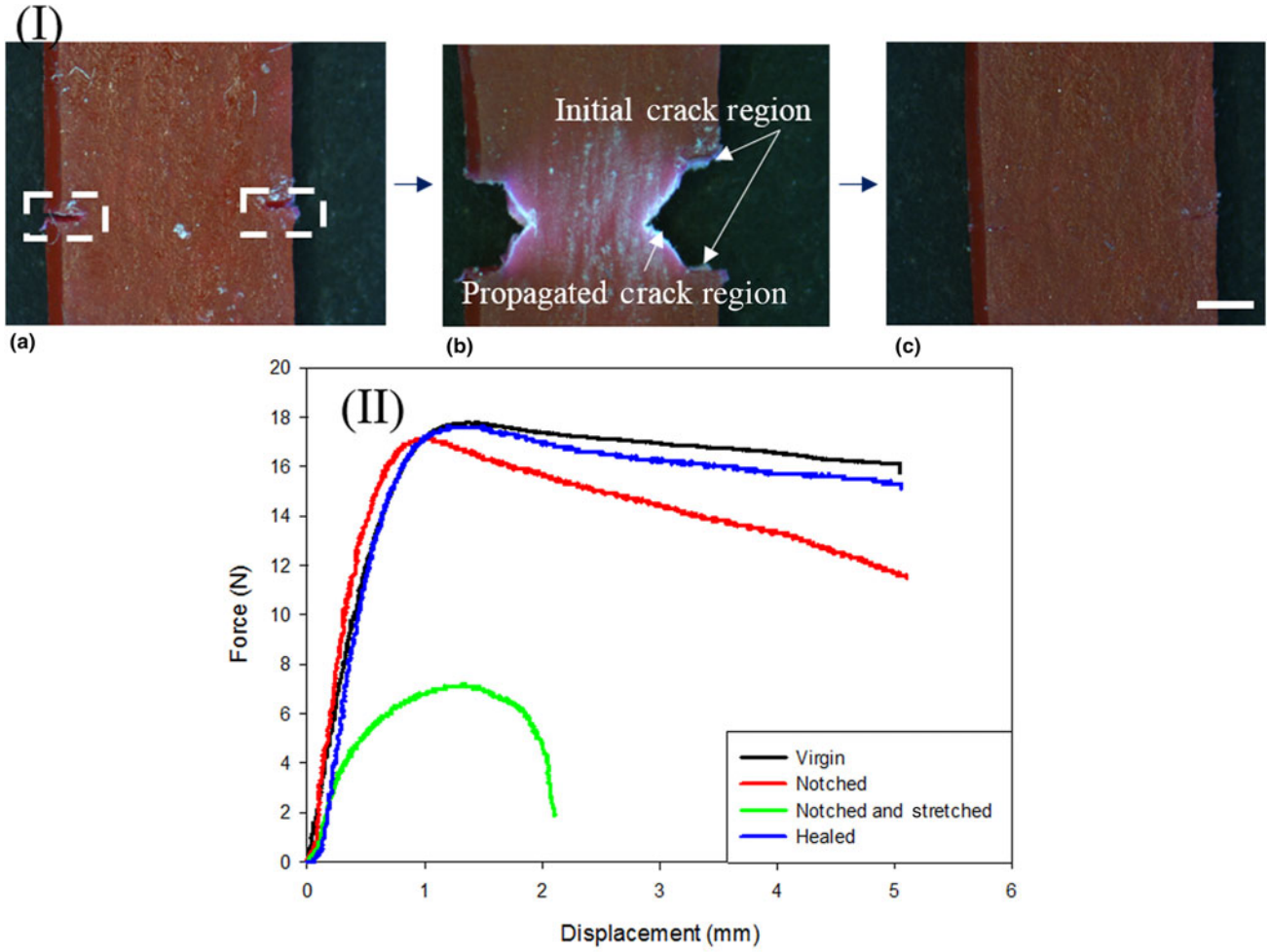


Figure 7. (I) Optical microscope images of a PVAc60:PCL40 film showing (a) notched sample, (b) crack propagated sample and (c) thermally mended sample (75 °C for 10 min). The sample was first notched using a custom-made cutter (a). The damage was then controllably propagated by stretching the notched sample (b). The damaged sample was then "self-healed" by heating isothermally at 75 °C for 10 min. Scale bar denotes 1 mm for all micrographs. (II) Force versus displacement curves for the virgin, notched damaged and healed states of a PVAc60:PCL40 film. The healed sample shows a profile almost identical to the virgin sample, indicating complete recovery of mechanical properties.

(89%) and failed at significantly lower displacement compared with virgin PVAc (see Fig. S14). We attribute this observation to the fact that even though the cracks were closed after heating the PVAc film, the crack surfaces were not rebonded and were not able to withstand the same stress as the virgin sample. While the present composite system showed promising SH abilities, further investigation is needed to reveal quantitative differences between the current approach and our prior miscible blend approach.[9]

Triple SM characterization of the hydrated film

The "plasticization" process of PVAc is a well-known process caused by an increase in free volume in the polymer, resulting from the presence of small molecules, such as water or other solvents. Increased free volume allows for more molecular movement, effectively reducing the T_g as evidenced in Fig. S9,[24,25] where the T_g is seen to reduce from ~45 to 16 °C. Upon hydration, the films (whether pure PVAc or PVAc:PCL composites) becomes elastomeric with a strain to failure above 500% (above the limits of our instrument) and a lower modulus, as shown in Fig. S15. Such a drastic response to a small amount of water uptake makes PVAc an excellent candidate for water-triggered SM polymers.[26] Dual SM of a dry composite film was first demonstrated by deforming a rectangular PVAc80:PCL20 sample [Fig. S16(A)] to a spiral shape (temporary shape) at 80 °C (20% being established as the optimal PCL loading level for triple SM properties in other systems[21,27–29]). Upon fixing in a freezer at −17 °C for 10 min, both PVAc and PCL phases were fixed by vitrification and crystallization, respectively [Fig. S16 (B)]. The fixed sample immediately recovered after being heated to 80 °C, as illustrated in Fig. S16(C). This is due to

https://doi.org/10.1557/mrc.2015.39 Published online by Cambridge University Press

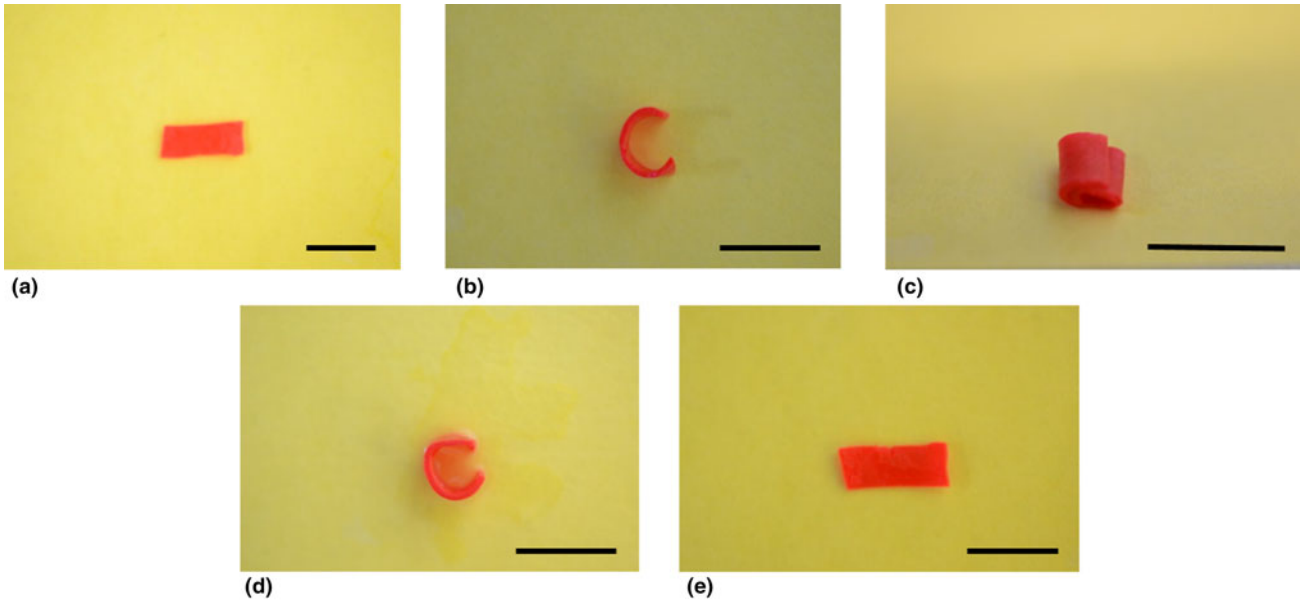


Figure 8. Triple shape memory demonstration of a hydrated PVAc80:PCL20 film showing (a) the permanent shape at RT, (b) temporary shape 1, a curled "C" shape, which was deformed in an 80 °C water bath and fixed by immersing in ice/water bath, (c) temporary shape 2, a rolled shape which was deformed in a water bath at RT and fixed by immersing in an ice/water bath, (d) recovered temporary shape 1, obtained by submerging in a water bath at RT for 10 min and (e) recovered permanent shape obtained by heating at 80 °C in water. All scale bars represent 1 cm.

the close vicinity of the PVAc T_g and PCL T_m. As such, an almost instantaneous recovery was observed by a simple heating step above them.

Triple SM materials can have two temporary shapes (A and B) programmed into them, allowing transition from shape (A) to shape (B) to shape (C),[21,27,28] where shape (C) is the permanent shape. Composites featuring two well-separated transitions exhibit triple SM properties.[21] Considering that the T_g of PVAc decreases to ~16 °C upon hydration (Fig. S9), the hydrated PVAc:PCL film had a T_g about 16 °C and a T_m about 55 °C, engendering it with triple SM characteristics, as shown in Fig. 8 for the PVAc80:PCL20 film. There, a flat rectangular sample (13 mm length, 5.2 mm width, and 0.9 mm thickness) was first curled to a "C" shape [temporary shape 1: Fig. 8(b)] in an 80 °C water bath and fixed immediately by quenching in ice/water bath. The sample was then rolled on itself in a water bath at RT and quenched in an ice/water bath as shown in Fig. 8(c). The sample recovered to its "C" shape [Fig. 8(d)] after immersing in water at RT for 10 min, and it quickly recovered back to its permanent-flat shape after heating the sample at 80 °C [Fig. 8(e)].

Conclusions

We have reported on the dual-electrospinning of two immiscible polymers that yields blended films with desirable mechanical functionality. Specifically PVAc and PCL solutions were dual-electrospun, yielding composites with good SH and SM properties using this novel, one-step method. The process is versatile and any pair of polymers that are each electrospinnable can be utilized to blend properties with fine-scale homogeneity. Given the simplicity of fabrication of composites, we envision mass production of SH and triple-shape films for applications that could range from building envelopes to food packaging.

Supplementary materials

For supplementary material for this article, please visit http://dx.doi.org/10.1557/mrc.2015.39

Acknowledgments

P. T. Mather acknowledges partial funding under NSF CMMI-1334658 and NSF EFRI-1435452. In addition, this investigation was partially supported under contract FA8651-13-C-0015 awarded by the Department of the Air Force to NEI Corporation.

References

1. D.Y. Wu, S. Meure, and D. Solomon: Self-healing polymeric materials: a review of recent developments. *Progr. Polym. Sci.* **33**, 479 (2008).
2. M. Kessler: Self-healing: a new paradigm in materials design. *Proc. Inst. Mech. Eng. G: J. Aerosp. Eng.* **221**, 479 (2007).
3. R.P. Wool: Self-healing materials: a review. *Soft Matter* **4**, 400 (2008).
4. S.R. White, N. Sottos, P. Geubelle, J. Moore, M.R. Kessler, S. Sriram, E. Brown, and S. Viswanathan: Autonomic healing of polymer composites. *Nature* **409**, 794 (2001).
5. Y.-L. Liu and T.-W. Chuo: Self-healing polymers based on thermally reversible Diels–Alder chemistry. *Polym. Chem.* **4**, 2194 (2013).

https://doi.org/10.1557/mrc.2015.39 Published online by Cambridge University Press

6. M. Kessler, N. Sottos, and S. White: Self-healing structural composite materials. *Compos. A: Appl. Sci. Manuf.* **34**, 743 (2003).
7. A. Lendlein and S. Kelch: Shape-memory polymers. *Angew. Chem. Int. Ed.* **41**, 2034 (2002).
8. P.T. Mather, X. Luo, and I.A. Rousseau: Shape memory polymer research. *Annu. Rev. Mater. Res.* **39**, 445 (2009).
9. E.D. Rodriguez, X. Luo, and P.T. Mather: Linear/network poly (ε-caprolactone) blends exhibiting shape memory assisted self-healing (SMASH). *ACS Appl. Mater. Interfaces* **3**, 152 (2011).
10. X. Luo and P.T. Mather: Shape memory assisted self-healing coating. *ACS Macro Lett.* **2**, 152 (2013).
11. A. Greiner and J.H. Wendorff: Electrospinning: a fascinating method for the preparation of ultrathin fibers. *Angew. Chem. Int. Ed.* **46**, 5670 (2007).
12. T. Subbiah, G. Bhat, R. Tock, S. Parameswaran, and S. Ramkumar: Electrospinning of nanofibers. *J. Appl. Polym. Sci.* **96**, 557 (2005).
13. Q.P. Pham, U. Sharma, and A.G. Mikos: Electrospinning of polymeric nanofibers for tissue engineering applications: a review. *Tissue Eng.* **12**, 1197 (2006).
14. A. Moghe and B. Gupta: Co-axial electrospinning for nanofiber structures: preparation and applications. *Polym. Rev.* **48**, 353 (2008).
15. Z.Y. Liu, D.D.L. Sun, P. Guo, and J.O. Leckie: An efficient bicomponent TiO_2/SnO_2 nanofiber photocatalyst fabricated by electrospinning with a side-by-side dual spinneret method. *Nano Lett.* **7**, 1081 (2007).
16. S. Madhugiri, A. Dalton, J. Gutierrez, J.P. Ferraris, and K.J. Balkus: Electrospun MEH-PPV/SBA-15 composite nanofibers using a dual syringe method. *J. Am. Chem. Soc.* **125**, 14531 (2003).
17. J.H. Park and P.V. Braun: Coaxial electrospinning of self-healing coatings. *Adv. Mater.* **22**, 496 (2010).
18. M. Yamaguchi, S. Ono, and M. Terano: Self-repairing property of polymer network with dangling chains. *Mater. Lett.* **61**, 1396 (2007).
19. D. Ferrer-Balas, M.L. Maspoch, A. Martinez, and O. Santana: On the essential work of fracture method: energy partitioning of the fracture process in iPP films. *Polym. Bull.* **42**, 101 (1999).
20. H. Koerner, G. Price, N.A. Pearce, M. Alexander, and R.A. Vaia: Remotely actuated polymer nanocomposites—stress-recovery of carbon-nanotube-filled thermoplastic elastomers. *Nat. Mater.* **3**, 115 (2004).
21. Q. Ge, X. Luo, C.B. Iversen, H.B. Nejad, P.T. Mather, M.L. Dunn, and H. Jerry Qi: A finite deformation thermomechanical constitutive model for triple shape polymeric composites based on dual thermal transitions. *Int. J. Solids Struct.* **51**, 2777 (2014).
22. M. Richard-Lacroix and C. Pellerin: Molecular orientation in electrospun fibers: from mats to single fibers. *Macromolecules* **46**, 9473 (2013).
23. A. Pedicini and R.J. Farris: Mechanical behavior of electrospun polyurethane. *Polymer* **44**, 6857 (2003).
24. W. Huang, B. Yang, L. An, C. Li, and Y. Chan: Water-driven programmable polyurethane shape memory polymer: demonstration and mechanism. *Appl. Phys. Lett.* **86**, 114105 (2005).
25. B. Yang, W. Huang, C. Li, and L. Li: Effects of moisture on the thermomechanical properties of a polyurethane shape memory polymer. *Polymer* **47**, 1348 (2006).
26. A.H. Torbati, R.T. Mather, J.E. Reeder, and P.T. Mather: Fabrication of a light-emitting shape memory polymeric web containing indocyanine green. *J. Biomed. Mater. Res. B: Appl. Biomater.* **102**, 1236 (2014).
27. A.H. Torbati, H.B. Nejad, M. Ponce, J.P. Sutton, and P.T. Mather: Properties of triple shape memory composites prepared via polymerization-induced phase separation. *Soft Matter* **10**, 3112 (2014).
28. H.B. Nejad, R.M. Baker, and P.T. Mather: Preparation and characterization of triple shape memory composite foams. *Soft Matter* **10**, 8066 (2014).
29. X. Luo and P.T. Mather: Triple-shape polymeric composites (TSPCs). *Adv. Funct. Mater.* **20**, 2649 (2010).

https://doi.org/10.1557/mrc.2015.39 Published online by Cambridge University Press